ISME

Iranian Journal of Mechanical Engineering
The Iranian Society of Mechanical Engineers
Research Paper
DOI: 10.30506/jmee.2020.113477.1197

Investigation of Welding Parameters Effects on Residual Stresses of Resistance Spot Welding of AZ31 Alloy

F. Nazari[*]
PhD

M. Sedighi[†]
Professor

D. Afshari[‡]
Assistant Professor

In this study, the effect of welding parameters on the residual stresses of resistance spot welding of AZ31 magnesium alloy was investigated. Resistance spot welding is a complicated multi-regime phenomenon which simulated by a developed electro-thermo-mechanical coupled finite element model. Interactions of parameters were determined using DOE method. The FE model was used to predict temperature changes, nugget growth, and the residual stresses distribution. The results of the simulation were validated with experimental data, based on the nugget diameter. The results showed that by increasing current and welding time the residual stresses are reduced. Increasing electrode force causes to increase residual stress but increasing holding time creates a peak in the amount of residual stresses. Also, evaluation of current sources revealed, in the same conditions, using direct current creates less residual stress than alternating current.

Keywords: Resistance spot welding, Residual stress, DOE, FE model, Magnesium alloy

1 Introduction

Nowadays the use of lightweight materials in the automobile industries and transportation is very important. So using magnesium alloys is rising because of lightweight and high ratio of strength to density. Resistance spot welding (RSW) is one of the fastest and oldest metal joining methods. RSW of magnesium alloys is widely used in many industrial applications especially in the automotive industry. RSW is multi-physics of electro-thermo-mechanical coupled phenomenon, and modeling this process can provide a base for more understanding the process performance and its results, especially to determine the effect of the process parameters on the residual stresses. Munitz et al. [1] were the first researchers that studied the RSW of magnesium alloys in (2002) and examined the possibility of RSW on Mg-AZ31 and Mg-AM50 alloys.

[*] Corresponding Author, PhD of Mechanical Engineering, Iran University of Science and Technology, Tehran, Iran f_nazari@alumni.iust.ac.ir
[†] Professor, Department of PMechanical Engineering, Iran University of Science and Technology, Tehran, Iran sedighi@iust.ac.ir
[‡] Assistant Professor, Department of Mechanical Engineering, University of Zanjan, Zanjan, Iran dafshari@znu.ac.ir
Receive : 2019/08/27 Accepted : 2020/10/04

Sun et al. [2] studied the effects of current and surface quality on the diameter and microstructure of the nugget and presented welding current higher than 15 KA is caused to appear hot cracking in the HAZ and nugget of magnesium sheets. Liu et al. [3-4] investigated the effects of current and surface quality on the RSW nugget and illustrated that by increasing the surface quality in the AZ31 sheets, the strength of nugget increases and damage of electrode tip face decreases. Shi et al. [5] studied the feasibility of using the cover plate in the RSW of mg sheets and revealed this technique can create larger nugget and higher tensile shear strength in the relatively low welding current. Hwang et al. [6] investigated the effect of DC and AC current sources in the RSW of magnesium alloy and presented DC current can create larger nugget with a higher strength than AC current. Afshari et al. [7] presented an approach in prediction of failure in resistance spot welded aluminum 6061-T6 and could calculate failure load in a quasi-static tensile test. Babu et al. [8] studied the effect of welding parameters on microstructure, solidification and nugget ductility of AZ31 alloy and presented the HAZ region has a dendritic microstructure and interfacial fracture occurs under the tensile and shear tests. Kramar et al. [9] evaluated the RSW of magnesium AZ61 and presented that growth the cracks along the grain boundaries is expected but with controlling the welding parameters it can be preventable. Min et al. [10] and Manladan et al. [11] investigated the methods for joining dissimilar magnesium-steel sheets by RSW and showed two methods of using the cover plate and RSW in welding brazing mode can be applicant for this purpose. Chabok et al. [12] studied the effect of pulse scheme on the residual stress and mechanical properties of resistance spot welded DP1000 steel and revealed double pulse welding (with low welding current) decreases mechanical properties of the weld. Afshari et al. [13] predicted residual stresses in RSW of aluminium sheets by neural network model and showed neural network model can positively predict residual stresses of RSW, also in another study [14] they investigated residual stresses in the RSW of AZ61 alloy and presented to reduce the residual stress in the welded zone maximum time and force with the minimum welding current are required. Simulation of resistance spot welding is an effective method to determine temperature, nugget diameter and residual stress at the welded zone. Ranjbar Nodeh et al. [15] Simulated residual stress of RSW by using FE modeling and verified by the X-ray method on the steel sheets. Sedighi et al. [16] investigated the effect of sheet thickness on residual stresses in RSW of aluminum sheets using a finite element model and showed residual stress of RSW increases with increasing the sheet thickness but it is controllable with controlling the welding parameters. Mikno and Bartnik [17] evaluated heating of electrodes during RSW in FEM calculations, and Mirzaahmadi et al. [18] investigated on the effect of material properties in the RSW simulation of magnesium alloy and presented thermal conductivity, electrical resistivity, and ECC have a significant effect on the nugget size. According to the literature, the residual stresses in the RSW of AZ31 magnesium alloys have not been investigated. In this research, the effect of welding parameters on the residual stresses in the RSW of AZ31 alloy has been evaluated. To study residual stresses in RSW, an electro-thermo-mechanical model was used and validated by using experimental results. Also, by using DOE analysis, the influence of welding parameters such as current, current time, force, holding time and current source on residual stresses in RSW of AZ31 were determined.

2 Materials and Method

2.1 Design of experiment

Experimental evaluation and simulation of RSW were conducted on the AZ31 sheet of magnesium with dimensions of 100mm×30mm×1mm that it is illustrated in figure (1). Tables (1) and (2) show mechanical and physical temperature-dependent properties of AZ31 alloy.

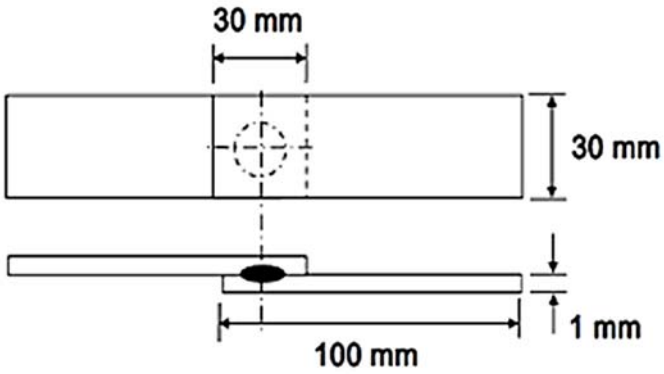

Figure 1 Geometry and dimensions of samples

Table 1 Mechanical properties of AZ31 magnesium alloy according to the temperature [19-20]

Temp. (°C)	25	100	150	200	243	300	400	450	
Young's modulus (GPa)	45	45	42.6	39.9	35.3	29.6	24.5	22	
Temp. (°C)	25	100	200	250	300	350	400	450	500
Yield straight (MPa)	154.8	145.9	137	125	122	95.2	68.9	51	38
Poisson's ratio	0.32								

Table 2 Physical properties of AZ31 magnesium alloy according to the temperature [19-20]

Temp. (°C)	25	100	200	300	428	538		
Thermal expansion ($^{10^{-5}}/_{\circ C}$)	2.6	2.64	2.7	2.79	2.84	2.89		
Temp. (°C)	25	100	200	300	400	430	500	668
Thermal conductivity ($w/m.k$)	84.7	90.5	95.8	98.4	104	107	95	137
Temp. (°C)	25	77	127	227	327	427	527	600
Electrical resistance ($\Omega.m.10^{-8}$)	10	11	11.5	13.5	15.2	17	18.7	20
Temp. (°C)	25	50	100	200	300	350	400	
Specific heat capacity ($j/Kg.k$)	1050	1100	1130	1170	1240	1290	1330	
Density (Kg/m^3)	1770							

Efficacy of each parameter on the residual stresses determined by using design of experiments DOE and Full Factorial method in the Minitab software. This method requires using the minimum and maximum values of each parameter. To characterize the allowable range of current intensity and welding time, a weld lobe which provided by Hwang et al. [6] was utilized. In this weld lobe (Figure 2), undersize weld or weld with insufficient strength was the lower limiting factor and the upper limiting factor was expulsion. In each section, experiments were designed in a way that the nugget always stands in the allowable range and weld be valid (no expulsion), and all of them were carried out in 200 Kg/cm^2 electrode force. The selected parameters are presented in Table (3).

2.2 Finite element model and boundary conditions

All boundary conditions of the finite element model including mechanical, electrical and thermal conditions have been presented in Figure (3). At the welding cycle, electrical current flows from the top surface of the upper electrode and after passing through the top and bottom contact areas between the electrode-sheet and sheet–sheet arrives at the lower face of the bottom electrode. The water temperature in the electrode channel has been assumed constant at 25ºC during all cycles of process. The surfaces that are in contact with air have 12 $Wm^{-2}K^{-1}$ convection coefficient. Also, room temperature has been assumed at 20ºC. In addition, the electrode force (P) has applied as a uniform pressure on the upper and lower electrodes.
To simulation of resistance spot welding process, used a two dimensional electro-thermo-mechanical coupled finite element model. This model has been created by writing subroutine in ANSYS software that utilized a direct couple method for design of this model and full Newton-Raphson solution method.

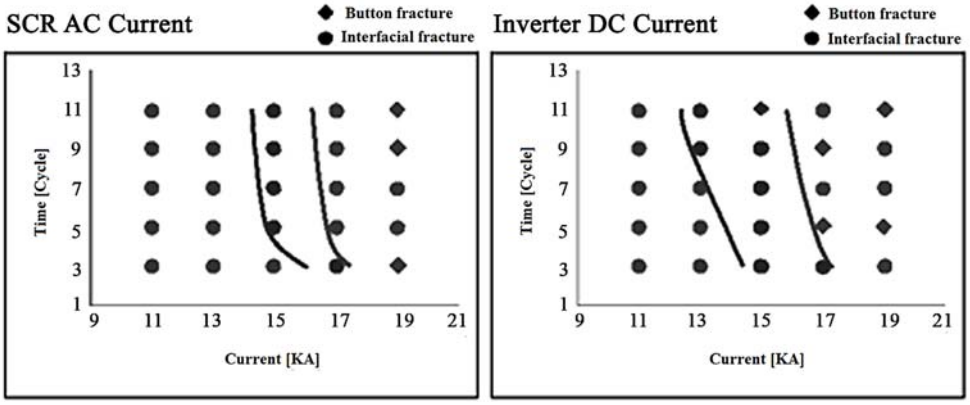

Figure 2 Weld lobe for 1 mm AZ31 magnesium sheet [6]

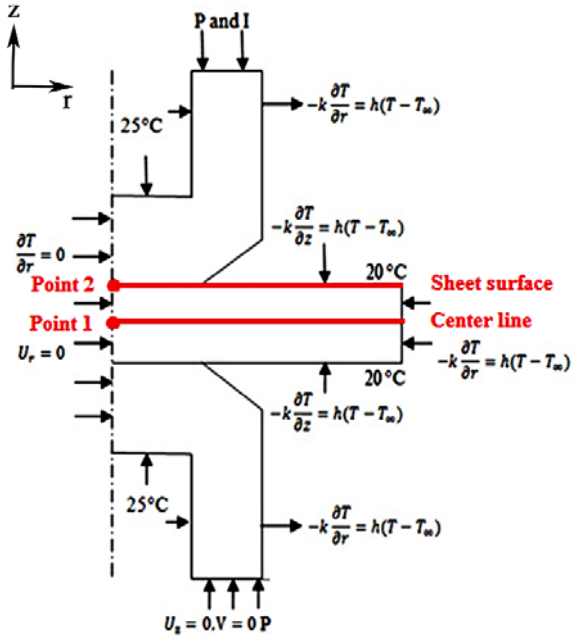

Figure 3 Boundary conditions of the finite element model

Table 3 selected parameters for numerical study

Experiment No.	Current (KA)	Current time (Cycle)	Force (KN)	Force time (Cycle)	Current source
1	13	7	2	6	AC
2	14	7	2	6	
3	15	7	2	6	
4	16	7	2	6	
5	17	7	2	6	
6	18	7	2	6	
7	16	4	2	6	
8	16	5	2	6	
9	16	6	2	6	
10	16	8	2	6	
11	16	9	2	6	
12	16	10	2	6	
13	16	7	1	6	
14	16	7	1.5	6	
15	16	7	2.5	6	
16	16	7	3	6	
17	16	7	3.5	6	
18	16	7	4	6	
19	16	7	2	3	
20	16	7	2	4	
21	16	7	2	5	
22	16	7	2	7	
23	16	7	2	8	
24	16	7	2	9	
25	14	7	2	6	DC
26	15	7	2	6	
27	16	7	2	6	
28	17	7	2	6	

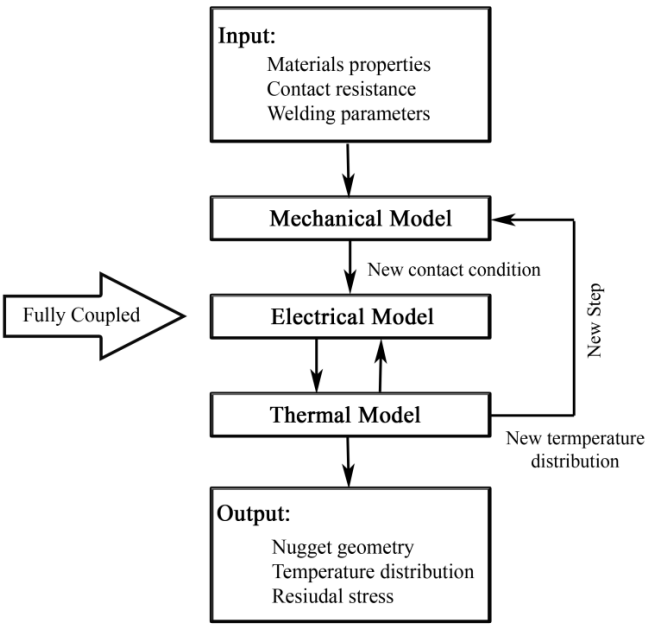

Figure 4 Resistance spot welding simulation algorithm

In mechanical and electro-thermal models respectively used Plane42 and Plane67 elements. To modeling contact in mechanical and electro-thermal models are used Canta171 and Target169 elements. After investigation of mesh sensitivity on the finite element model, selected 0.2 and 0.5 mm mesh size for sheets and electrodes and created 2100 elements on the model. Because, thermal, electrical and mechanical properties of materials change with temperature changes, time of 0.001 Second is considered to refresh and update all of the material properties. The simulation algorithm is shown in figure (4).

2.3 Theoretical background

Resistance spot welding is a complex process that involved thermal, electrical, mechanical and metallurgical factors. In order to model this process need to extract each phenomenon equations. For the simulation, the process is considered to be axisymmetric and the equations used in this model are two-dimensional in the cylindrical coordinates. Equation (1) represents the governing equation on electrical potential (φ). In this equation r is radial distance; z is the distance along the axis of cylindrical coordinate and σ is the electrical conductance. Solving the equation presents electrical potential distribution in the model.

$$\frac{\partial}{\partial r}\left(\sigma\frac{\partial\varphi}{\partial r}\right)+\frac{\sigma}{r}\frac{\partial\varphi}{\partial r}+\frac{\partial}{\partial z}\left(\frac{\partial\varphi}{\partial z}\right)=0 \tag{1}$$

The thermal model includes the dynamic investigation of temperature resulting from the changes of electrical current, heat generation and also heat transfer by conduction and convection. This model has been expressed by equations (2) and (3) [14]; where q is the generated heat as a result of electrical potential and ρ is density of the material. Also, R, C, and k are respectively resistance, thermal capacity, and thermal conductance of the sheet which all of them are temperature-dependent parameters. In these relations, T and t denote the temperature distribution and the time, respectively.

$$q=\frac{\varphi^2 t}{R} \tag{2}$$

$$\frac{\partial}{\partial r}\left(k\frac{\partial T}{\partial r}\right)+\frac{k}{r}\left(\frac{\partial T}{\partial r}\right)+\frac{\partial}{\partial z}\left(\frac{\partial T}{\partial z}\right)+\dot{q}=\rho c\frac{\partial T}{\partial t} \tag{3}$$

To calculate the stress and strain in the FE model the following equations have been used. In equations (4-6), H is the hardness matrix, ϕ is the displacement vector, f is the force vector, {σ} is the stress vector, [D] is an elastic-plastic matrix, {ε} is strain vector, [D^e] is an elastic matrix and {α} is thermal expansion coefficient.

$$H.\phi+f=0 \tag{4}$$

$$d\{\sigma\}=[D]d\{\varepsilon\}-\{C\}dT \tag{5}$$

$$\{c\}=-\left[D^e\right]\left(\{\alpha\}+\frac{\partial\left[D^e\right]^{-1}}{\partial T}\{\sigma\}\right) \tag{6}$$

To define heat transfer by conduction between the contacts surfaces the equation (7) has been used where Q is transferred heat between the contacts surfaces, h is thermal contact conductance, T_t and T_c are the temperatures at the contact points on the contact and target surfaces.

$$Q=h\times\left(T_t-T_c\right) \tag{7}$$

Equation (8) has been utilized to compute the thermal contact conductance (h). In this equation Ks is the harmonic mean thermal conductivity of surface, m is the effective mean absolute

asperity slope of the interface, σ is the effective RMS surface roughness of the contacting asperities and P and E', respectively, are the electrodes pressure and equivalent elastic modulus [21].

$$h = 1.25 \times \left(\frac{\sqrt{2}P}{mE'}\right)^{0.94} \times \frac{mK_s}{\sigma} \tag{8}$$

The electrical properties of the two contact surfaces have been defined by equation (9) where J is electrical current density, ECC is electric contact conductance and V_c and V_t are voltages at the contact points on the contact and target surfaces.

$$J = ECC \times \left(V_t - V_c\right) \tag{9}$$

To define ECC equations (10) and (11) have been used which R is electrical resistance, L is elements length, A is the area of the contact zone and σ_Y is the yield stress [22].

$$R\left(T\,^{\circ}C\right) = \frac{A}{l} \times R\left(20^{\circ}C\right) \times \sqrt{\frac{\sigma_{Y\,(T\,^{\circ}C)}}{\sigma_{Y\,(20^{\circ}C)}}} \tag{10}$$

$$ECC = \frac{1}{R\left(T\,^{\circ}C\right)} \tag{11}$$

Also, the alternative current has been calculated by equation (12) that I_m is maximum current intensity in Ampere, fr is a frequency in Hertz and t is a time in Second.

$$I = I_m \sin\left(2\pi fr\, t\right) \tag{12}$$

3 Results and discussions

To validate the finite element model, the simulation results have been compared with the experimental results obtained by Hwang et al. [6] on the AZ31 sheet with 1 mm thickness. The experiments performed in 9 Cycle current time, 2000 N electrode force and four levels of current, and investigated two DC and AC with 60 Hz frequency current sources. The simulation results compared with experimental data only base on nugget diameter because there is no information about residual stresses of Magnesium resistance spot welding. As can be observed in figure (5), the simulation result has a good agreement with the experimental result.
In Table (4), the simulation results have compared with experimental data and expressed the percentage of errors.

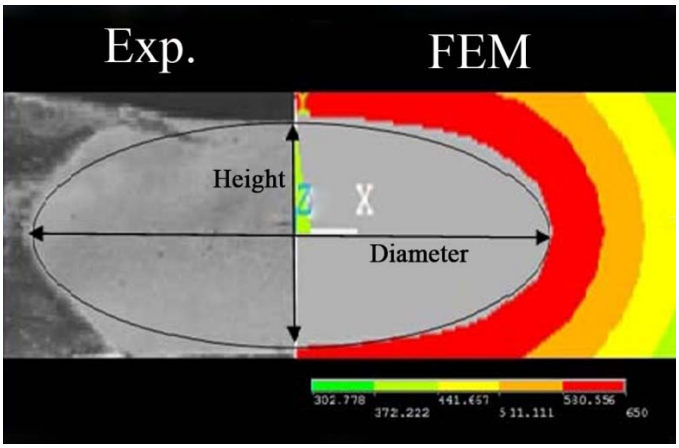

Figure 5 Comparing simulation and experiment nugget shape

Table 4 Comparing simulation and experimental nugget diameter

Current (KA)	Alternative current (AC)			Direct current (DC)		
	Simulation (mm)	Experiment (mm)	Error%	Simulation (mm)	Experiment (mm)	Error%
13	3.5	3.6	2.8	3.8	3.9	2.5
15	3.8	4	5	4.28	4.4	2.7
17	4.56	4.6	0.8	5.06	5	1.2
19	5.4	5.8	6.8	5.8	6	3.3
Average error (%)			3.8	Average error (%)		2.4

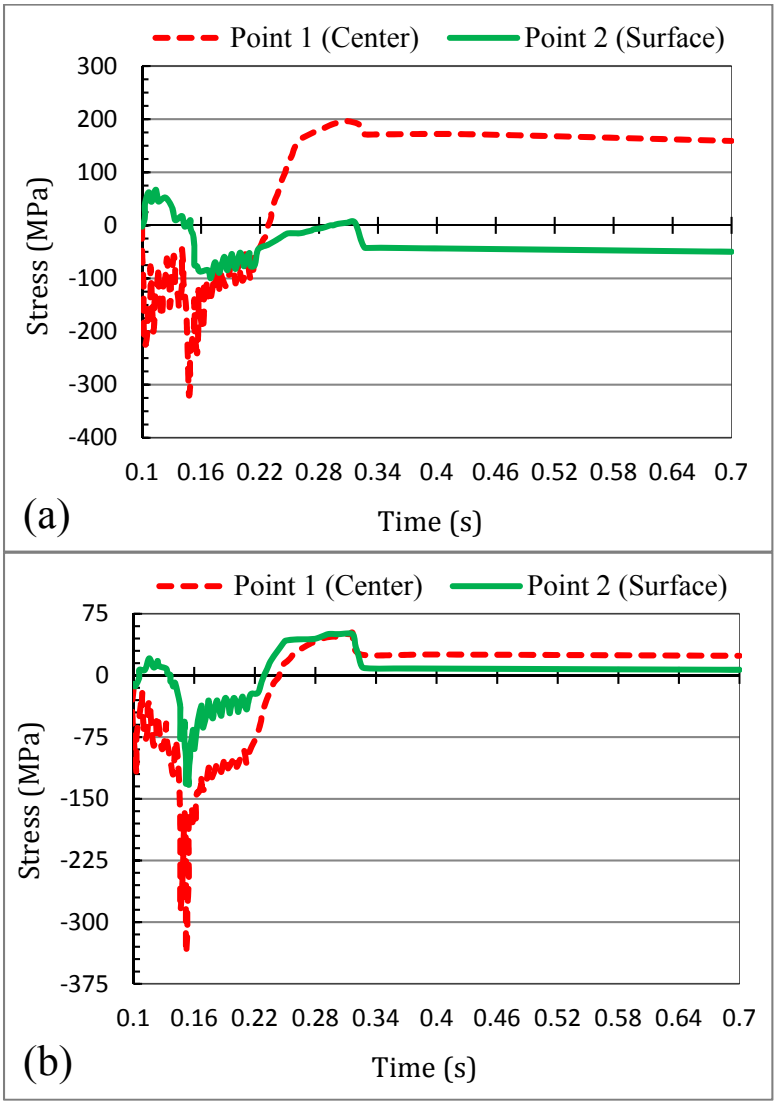

Figure 6 Changes of residual stress along (a) nugget radius (r-direction), (b) sheet thickness (z-direction)

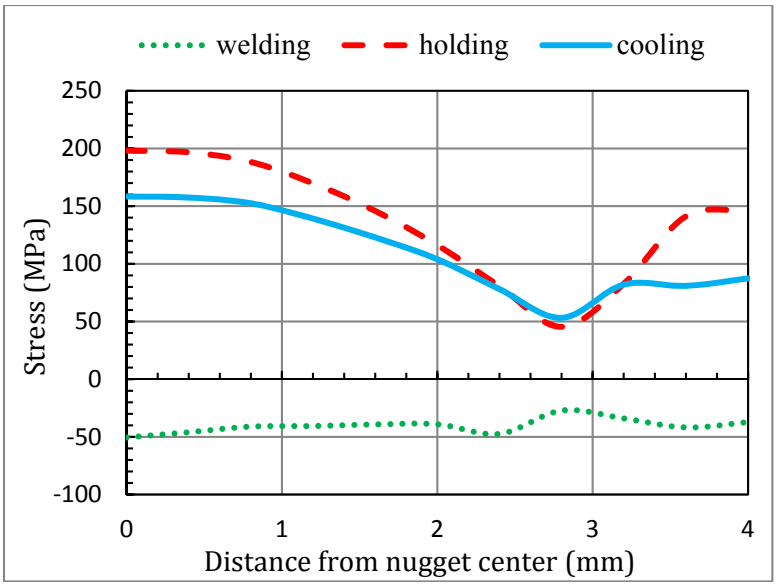

Figure 7 Stress in the r-direction according to distance from the nugget center

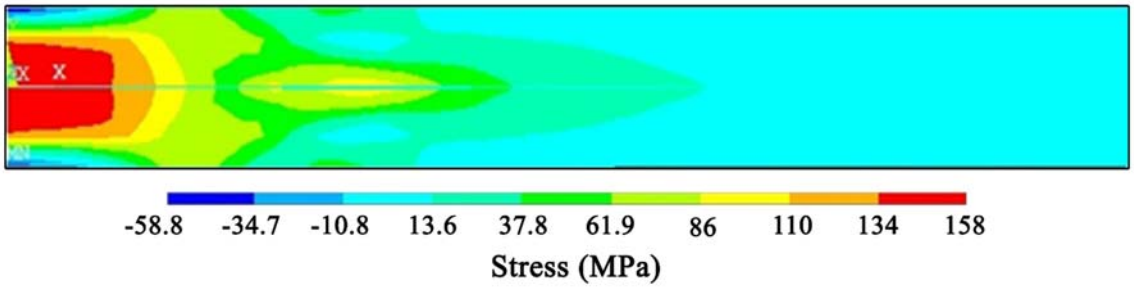

Figure 8 Contour of residual stress in the r-direction (nugget radius) after cooling cycle

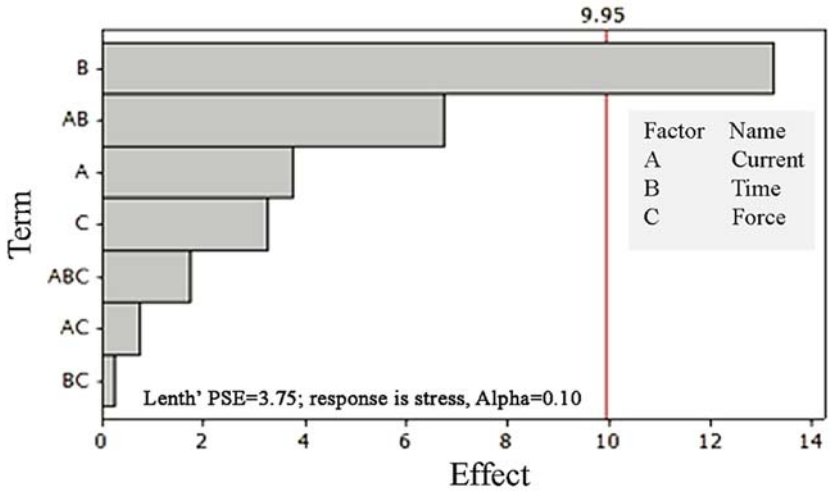

Figure 9 The effect of RSW parameters on the residual stresses

At the beginning of the process, the electrodes apply force on the sheets and then electrical current flows and temperature rises. The weld area tends to have expansion but base metal is cold and resists against increasing the volume that causes to create compressive stress in the welded area and tensile stress in the base metal. When the current be off, heated and melted zones are cooled down and this process will be reversed. So by cooling, the weld zone tends to shrinkage and the base metal, which warmed because of heat transfer, tends to expansion.

This procedure causes to create tensile stress in nugget and compressive stress in base metal and sheet surface. Figure (6) illustrated stress changing procedure due to the welding process in the nugget center (point 1) and sheet surface (point 2). As be seen in this figure, stress value along z-direction is much less than the stress along r direction. Point 1 and point 2 have been indicated in figure (3). Investigation of residual stress results indicated the maximum residual stress occurs at the nugget center and by moving along nugget radius the residual stresses diminish. Figure (7) illustrates changing stress at the nugget center during the process and figure (8) shows the distribution of residual stresses at the end of the process.

According to the design of experiment (DOE), evaluating the effect of RSW parameters on residual stresses indicated current time and interaction of current and current time have a great influence on the residual stress. Figure (9) shows the effect of different parameters on the residual stresses. According to the results, by increasing current or current time, more heat generates and the nugget size will enlarge consequently. After separating the electrodes, cooling time has been longer because of the higher heat stored in the welding zone. So it causes to create lower residual stresses in the specimen. Figure (10) illustrates the effect of welding current and time on the residual stresses in the r direction.

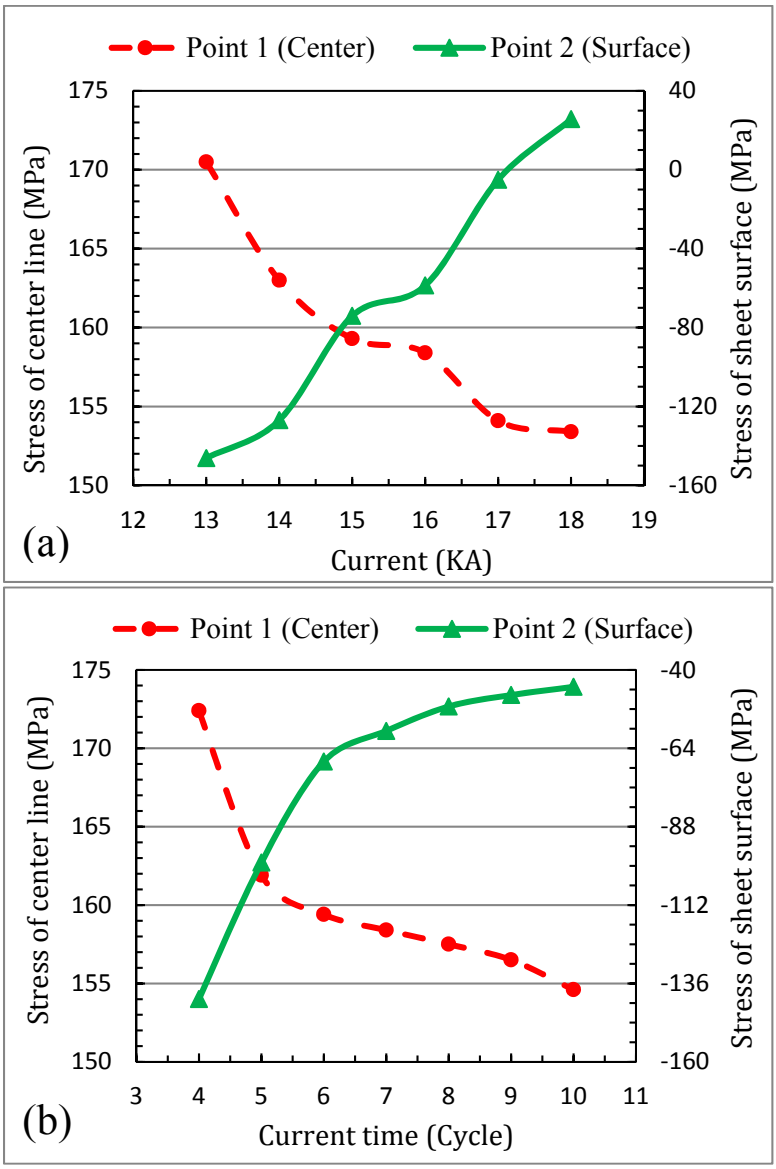

Figure 10 Effect of (a) welding current and (b) current time on the residual stresses

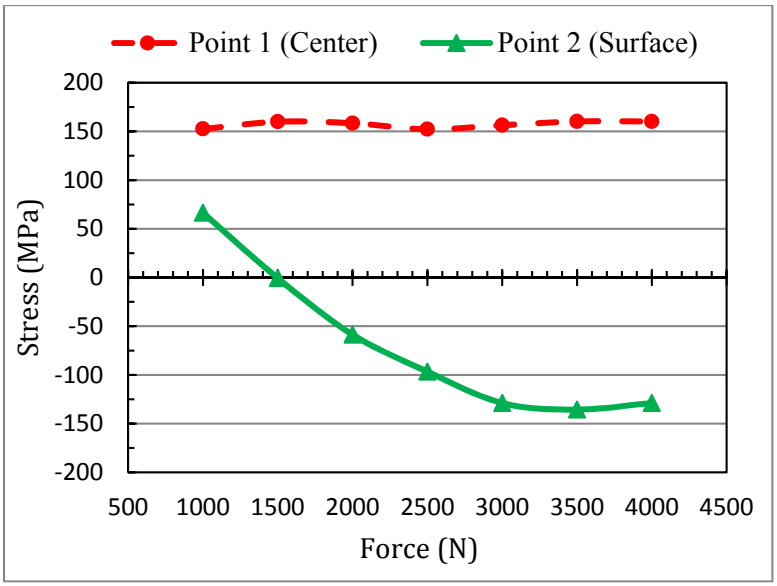

Figure 11 Effect of electrode force on residual stress in the r-direction

As shown in figure (11), by increasing electrode force, compressive residual stress increases at the sheet surface. But the effect of electrode force on residual stresses is small at the interface of two sheets. If electrode force increases, direct contact of electrode and sheet surface increase and cooling rate of sheet surface increases. This fact can explain why the higher residual stress is observed at the surface. The effect of holding time on residual stresses is shown in figure (12). The maximum residual stress occurs at 4 Cycle of holding time and then, residual stresses decrease via increasing holding time. It may be able to explain that via enhancement of holding time up to 4 Cycle causes to increase heat transfer and therefore makes higher residual stress in the welding domain. But increasing holding time more than 4 Cycle causes to high temperature reduction via electrodes. Because of this, compressive stresses that created due to compressive force stabilize. So, by unloading force didn't eliminate compressive stresses that cause to neutralize some of the tensile residual stresses.

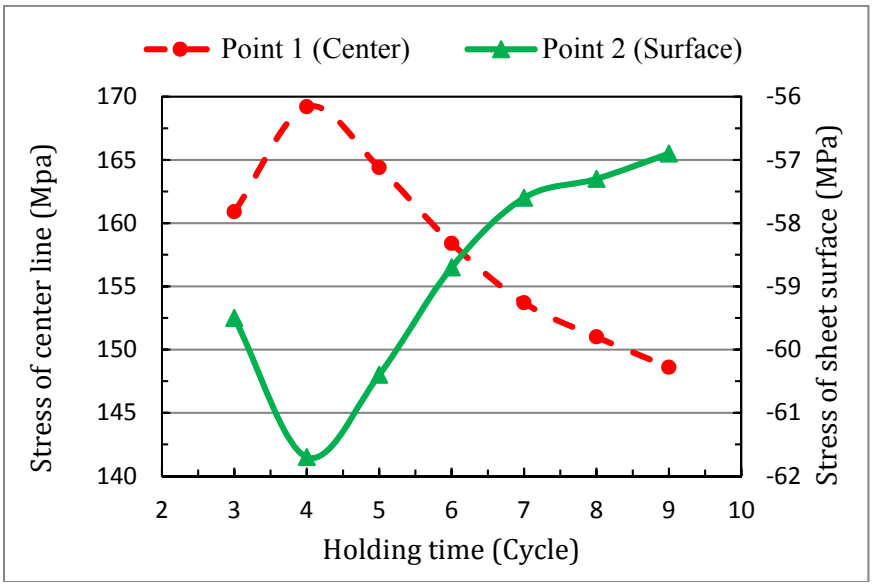

Figure 12 Effect of holding time on residual stresses along the radius

According to DOE results can be noted that the interaction of current-time has the most effective effect on the residual stresses than current-force, time-force or current-time-force. As illustrated in figure (13), the maximum residual stress occurred in the nugget center due to simultaneous reduction in the current and current time. Investigation of current source demonstrates direct current (DC) always creates less residual stress than alternative current (AC). Because of DC generates more heat flux in the welding zone than AC. Consequently, the nugget was bigger and longer cooling time needs for reaches to the ambient temperature that causes to reduce the residual stresses. Created residual stress at the nugget center (Point 1) by using DC and AC current sources is shown in figure (14).

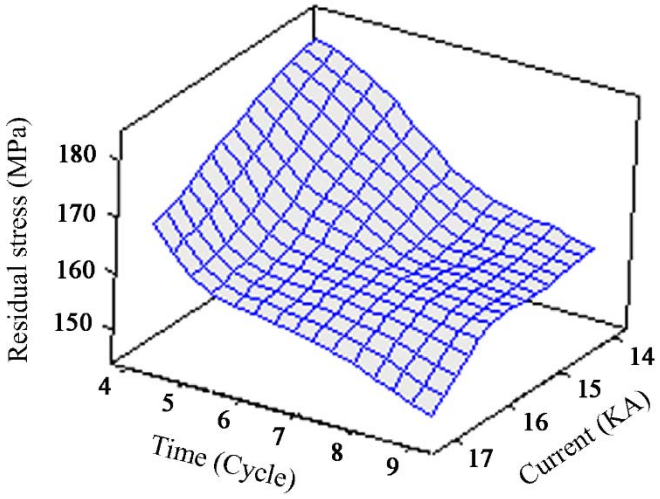

Figure 13 Effect of interaction current and current time on the maximum of residual stress

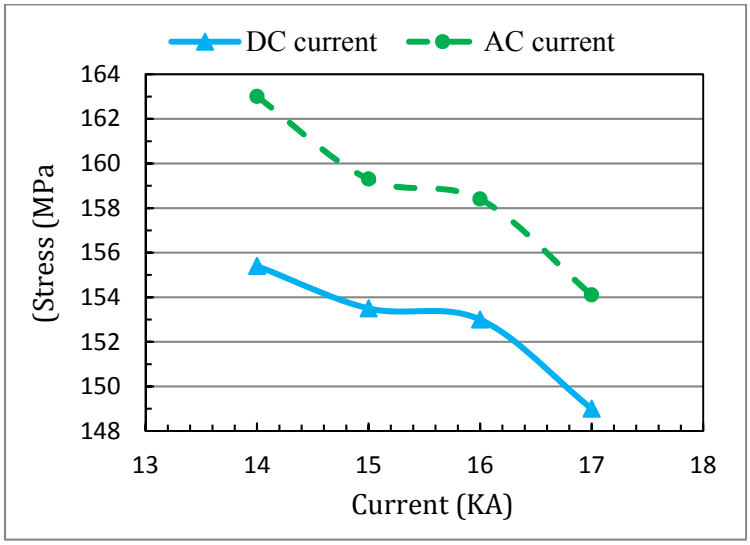

Figure 14 Created residual stress in the r-direction by using both DC and AC current source

4 Conclusions

In this research by developing an electro-thermo-mechanical coupled finite element model, the effect of welding parameters on the residual stresses in the resistance spot welding of AZ31 magnesium alloy has been investigated. According to the results, the thermal gradient creates maximum compressive residual stress at the sheet surface and maximum tensile residual stress is formed at the nugget center. Also, with moving away from the nugget center, the residual stresses decrease in the radius direction. Based on the obtained results from the simulation and

DOE analysis, the current time and interaction of current-current time have the most effects on residual stresses. By increasing current and current time, the residual stresses along the radius in both of nugget and sheet surface are reduced. Increasing electrode force causes to increase compressive residual stress at the sheet surface but it doesn't have a significant effect at the nugget region. Investigation of current sources indicated that at the same conditions, the direct current is better than alternating current because of creation larger nugget with lower residual stresses in the welding zone.

References

[1] Munitz, A., Kohn, G., and Cotler, C., "Resistance Spot Welding of Mg-AM50 and Mg-AZ91D Alloys", The Minerals, Metals & Materials Society, Vol. 1, pp. 303-307, (2002).

[2] Sun, D.Q., Lang, B., Sun, D.X., and Li, J.B., "Microstructures and Mechanical Properties of Resistance Spot Welded Magnesium Alloy Joints", Materials and Science Engineering A, Vol. 460-461, pp. 494-498, (2007).

[3] Liu, L., Zhou, S.Q., Tian, Y.H., Feng, J.C., Jung, J.P., and Zhou, Y.N., "Effects of Surface Conditions on Resistance Spot Welding of Mg Alloy AZ31", Science and Technology of Welding and Joining, Vol. 14, pp. 356-361, (2009).

[4] Liu, L., Xiao, L., Feng, J.C., Tian, Y.H., Zhou, S.Q., and Zhou, Y., "Resistance Spot Welded AZ31 Magnesium Alloys, Part II: Effects of Welding Current on Microstructure and Mechanical Properties", Metall. Mate. Trans. A, Vol. 41, pp. 2641-2650, (2010).

[5] Shi, H., Qiu, R., Zhu, J., Zhang, K., Yu, H., and Ding, G., "Effects of Welding Parameters on the Characteristics of Magnesium Alloy Joint Welded by Resistance Spot Welding with Cover Plates", Materials and Design, Vol. 31, pp. 4853-4857, (2010).

[6] Hwang, I.S., Kim, D.C., and Kang, M.J., "Inverter DC Resistance Spot Welding of Magnesium Alloy AZ31", Archives of Materials and Science Engineering, Vol. 48, pp. 112-117, (2011).

[7] Afshari, D., Sedighi, M., Barsoum, Z., and Peng, R.L., "An Approach in Prediction of Failure in Resistance Spot Welded Aluminum 6061-T6 under Quasi-static Tensile Test", Proceedings of the Institution of Mechanical Engineers, Part B: Journal of Engineering Manufacture, Vol. 226, No. 6, pp. 1026-1032, (2012).

[8] Babu, N.K., Brauser, S., Rethmeier, M., and Cross, C.E., "Characterization of Microstructure and Deformation Behavior of Resistance Spot Welded AZ31 Magnesium Alloy", Materials and Science Engineering A, Vol. 549, pp. 149-156, (2012).

[9] Kramar, T., Vondrous, P., Kolarikova, M., Kovanda, K., Kolarik, L., and Ondruska, M., "Resistance Spot Welding of Magnesium Alloy AZ61", MM Science Journal, pp. 596-599, (2015).

[10] Min, D., Yong, Z., and Jie, L., "Dissimilar Spot Welding Joints of AZ31-443 Ferritic Stainless Steel with Cover Plate", The International Journal of Advanced Manufacturing Technology, Vol. 85, pp. 1539-1545, (2016).

[11] Manladan, S.M., Yusof, F., Ramesh, S., Zhang, Y., Luo, Z., and Ling, Z., "Microstructure and Mechanical Properties of Resistance Spot Welded in Welding-brazing Mode and Resistance Element Welded Magnesium Alloy/Austenitic Stainless Steel Joints", Journal of Materials Processing Technology, Vol. 250, pp. 45-54, (2017).

[12] Chabok, A., Ellen, V.D.A., Indranil, B., Jeff, D.H., and Yutao, P., "Effect of Pulse Scheme on the Microstructural Evolution, Residual Stress State and Mechanical Performance of Resistance Spot Welded DP1000-GI Steel", Science and Technology of Welding and Joining, Vol. 23, No. 8, pp. 649-658, (2018).

[13] Afshari, D., Sedighi, M., Karimi, M.R., and Barsoum, Z., "Prediction of Residual Stresses in Resistance Spot Weld", Aircraft Engineering and Aerospace Technology, Vol. 88, No. 4, pp. 492-497, (2016).

[14] Afshari, D., Mirzaahamdi, S., and Barsoum, Z., "Residual Stresses in Resistance Spot Welded AZ61 Mg Alloy", CMES-Computer Modeling in Engineering & Sciences, Vol. 118, No. 2, pp. 275-290, (2019).

[15] Ranjbar Nodeh, I., Serajzadeh, S., and Kokabi, A.H., "Simulation of Welding Residual Stresses in Resistance Spot Welding, FE Modeling and X-Ray Verification", Journal of Materials Processing Technology, Vol. 205, pp. 60-69, (2008).

[16] Sedighi, M., Afshari, D., and Nazari, F., "Investigation of the Effect of Sheet Thickness on Residual Stresses in Resistance Spot Welding of Aluminum Sheets", Proceedings of the Institution of Mechanical Engineers Part C: J. Mechanical Engineering Science, Vol. 232, No. 4, pp. 621-638, (2016).

[17] Mikno, Z., and Bartnik, Z., "Heating of Electrodes During Spot Resistance Welding in FEM Calculations", Archives of Civil and Mechanical Engineering, Vol. 16, pp. 86-100, (2016).

[18] Mirzaahmadi, S., Afshari, D., and Barsoum, Z., "Investigating the Effect of Material Properties on Simulation of Mg Alloy Resistance Spot Welding Process", Iranian Journal of Manufacturing Engineering, Vol. 6, No. 1, pp. 53-60, (2019).

[19] Yang, H., Huang, L., and Zhan, M., "Magnesium Alloys Design, Processing and Properties", Frank Czerwinski (Editor), Hot Forming Characteristics of Magnesium Alloy AZ31 and Three-dimensional FE Modeling and Simulation of the Hot Splitting Spinning Process, Intech ISSN: 978-953-307-520-4, pp. 367-388, (2011).

[20] Ding-Fei, Z.H., Qing-Wei, D., Lin, F., and Jun-Ping, Z.H., "Simulation and Confirmatory Experiment on Rolling of Magnesium Alloy Sheets with Temperature Gradient", The Chinese Journal of Nonferrous Metals, Vol. 21, pp. 185-190, (2011).

[21] Yovanovich, M.M., Culham, J.R., and Teertstra, P., "Calculating Interface Resistance", Journal of Electronic Cooling, Vol. 3, pp. 24-29, (1997).

[22] Cha, B.W., and Na SJ, A., "Study on the Relationship between Welding Conditions and Residual Stress of Resistance Spot Welded 304-Type Stainless Steels", Journal of Manuf. Systems, Vol. 22, pp. 181-189, (2003).

Nomenclature and Abbreviations

p	Electrode pressure
r	Radial distance
σ	Electrical conductance
ρ	Material density
C	Thermal capacity
T	Temperature
H	Hardness matrix
f	Force vector
$[D]$	Elastic-plastic matrix
$[D^e]$	Elastic matrix
Q	Transferred heat between surfaces
Ks	Harmonic mean thermal conductivity
J	Electrical current density
V	Voltages at the contact points
A	Area of the contact zone
I_m	Maximum current intensity
φ	Electrical potential
z	Vertical axis of cylindrical coordinate
q	Generated heat
R	Electrical resistance
k	Thermal conductance
t	Time
ϕ	Displacement vector
$\{\sigma\}$	Stress vector
$\{\varepsilon\}$	Strain vector
$\{\alpha\}$	Thermal expansion coefficient
h	Thermal contact conductance
E'	Equivalent elastic modulus
ECC	Electric contact conductance
L	Elements length
σ_Y	Yield stress
fr	Frequency